Inorg. Chem. **2004**, *43*, 1865–1873

Intermolecular Magnetic Couplings in the Dinuclear Copper(II) Complex μ-Chloro-μ-[2,5-bis(2-pyridyl)-1,3,4-thiadiazole] Aqua Chlorocopper(II) Dichlorocopper(II): Synthesis, Crystal Structure, and EPR and Magnetic Characterization

Fouad Bentiss,[†] Michel Lagrenée,[†] Olivier Mentré,[†] Pierre Conflant,[†] Hervé Vezin,[‡] Jean Pierre Wignacourt,*[,†] and Elizabeth M. Holt[§]

Laboratoire de Cristallochimie et Physicochimie du Solide, CNRS UMR 8012, ENSCL, BP 108, F-59652 Villeneuve d'Ascq Cedex, France, Laboratoire de Chimie Organique et Macromoléculaire, CNRS UMR 8009, USTL, Bât C3, F-59655 Villeneuve d'Ascq Cedex, France, and Department of Chemistry, Oklahoma State University, Stillwater, Oklahoma 74078

Received April 14, 2003

μ-Chloro-μ-[2,5-bis(2-pyridyl)-1,3,4-thiadiazole] aqua chlorocopper(II) dichlorocopper(II) is the first characterized dimeric complex of a transition metal and this hetero ligand [$C_{12}H_{10}Cl_4Cu_2N_4OS$; triclinic; space group $P\bar{1}$; a = 9.296(3) Å, b = 9.933(3) Å, c = 10.412(3) Å; α = 79.054(5)°, β = 82.478(6)°, γ = 67.099(5)°; Z = 2 at room temperature]. The Cu(II) ions are bridged by the N–N thiadiazole bond and a chloride ion [Cu1–Cu2 = 3.7800(8) Å]. Thermogravimetric analysis shows this structure to be stable at temperatures up to 348 K. At higher temperatures, the successive loss of a water molecule and one chloride of the dimeric unit is identified. From room temperature to 125 K, half of the Cu^{2+} ions are progressively engaged in intermolecular dinuclear antiferromagnetic exchanges, while the other half remain paramagnetic. At lower temperatures, both susceptibility and electron paramagnetic resonance measurements show the paramagnetic-only couplings of this half of the Cu^{2+} ions, involving a singlet ground state for interacting Cu^{2+}. This unusual behavior has been satisfactorily explained on the basis of intermolecular Cu–Cu interactions (J = –180 cm^{-1}), involving the magnetic d_{z^2} orbital perpendicular to the molecular plane, on which are seen the conjugate effects of the bridging chloride and the planar thiadiazole. It is noteworthy that the behavior of the title compound is original, compared to the systematic in-plane intramolecular antiferromagnetic coupling of other thiadiazole-containing binuclear complexes.

Introduction

There is interest in the dimeric metal complexes with close metal−metal contacts and appropriate bridging atoms for their magnetic properties.[1−7] These properties may be modified by the character of the bridging species and the geometry of the metal atoms and bridging species. Four tetraheteroatom derivatives of 1,2-diazoles with *o*-pyridine substitution at the 3 and 5 positions have been of interest for such applications (Figure 1). These ligands form complexes with appropriate transition metals (M) displaying intramolecular magnetic exchanges in the dinuclear compounds. Magnetic exchange involving the M−N═N−M bridge has been postulated to result from a σ-overlap superexchange pathway involving σ electrons of the heterocycle. Crossover from one magnetic behavior to the other is invoked by control of the structural

* Author to whom correspondence should be addressed. E-mail: wignacourt@ensc-lille.fr. Tel: +33-320-436-542. Fax: +33-320-436-814.
[†] Laboratoire de Cristallochimie et Physicochimie du Solide, Lille University.
[‡] Laboratoire de Chimie Organique et Macromoléculaire, Lille University.
[§] Oklahoma State University.

(1) Tang, J. K.; Wang, H. M.; Cheng, P.; Liu, X.; Liao, D. Z.; Jiang, Z. H.; Yan, S. P. *Polyhedron* **2001**, *20* (7 and 8), 675−680.
(2) Tang, J. K.; Wang, H. M.; Cheng, P.; Liu, X.; Liao, D. Z.; Jiang, Z. H.; Yan, S. P. *Polym. J. Chem.* **2000**, *74* (11), 1651−1654.
(3) Gabryszewski, M. I.; Wieczorek, B. *Spectrosc. Lett.* **2000**, *33* (1), 23 and 24.
(4) Ferrer, S.; Van Koningsbruggen, P. J.; Haasnoot, J. G.; Reedjijk, J.; Kooijman, H.; Spek, A. L.; Lezama, L.; Arif, A.; Miller, J. S. *J. Chem. Soc., Dalton Trans.* **1999**, *23*, 4269−4276.
(5) Liu, J. C.; Fu, D. G.; Zhuang, J. Z.; Duan, C. Y.; You, X. Z. *J. Chem. Soc., Dalton Trans.* **1999**, *14*, 2337−2342.
(6) Singh, V. K.; Sinha, R.; Kant, R.; Sinha, B. K. *Asian J. Chem.* **1998**, *10* (3), 532−535.
(7) Van Koningsbuggen, P. J.; Haasnoot, J. G.; Vreugdenhil, W.; Reedijk, J.; Kahn, O. *Inorg. Chim. Acta* **1995**, *239* (1 and 2), 5−12.

10.1021/ic030128s CCC: $27.50
Published on Web 02/25/2004

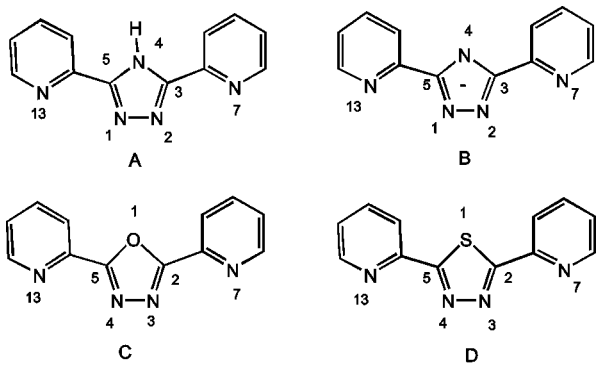

Figure 1. Scheme of the four related ligands: (a) 3,5-bis(2-pyridyl)-4*H*-1,2,4-triazole, (b) 3,5-bis(2-pyridyl)-1,2,4-triazolate ion, (c) 2,5-bis(2-pyridyl)-1,3,4-oxadiazole, (d) bptd.

parameters such as the coplanarity of metal- and heteroatom-containing ligands and the magnitude of the M−N═N angles. A review of the literature shows that neutral forms of such ligands form monometallic complexes with transition metals, whereas the anionic form leads to dimeric complexes. 1,3,4-Oxadiazoles with such substitution (bpo; Figure 1C) are neutral ligands. They normally form monomeric complexes without metal−metal interactions.[8−10] The only reported example of a multimetal complex with bpo is the polymeric species $[Cu(bpo)Cl_2]_\infty$, in which successive metal centers are bridged by the tetradentate ligand.[8]

We have recently reported the synthesis and characterization of monomeric complexes of Co(II), Ni(II), and Cu(II) with the 2,5-bis(2-pyridyl)thiadiazole derivative (bptd; Figure 1D).[11] There are no other reports of the structures of solid-state complexes of this neutral bptd ligand.

1,2,4-Triazole with *o*-pyridine substitution at the 3 and 5 positions (bpt) may be used as a ligand in neutral or anionic form. When one of the three nitrogen atoms of the aromatic triazole ring bears a substituent, the ligand is neutral (Figure 1A). When this substituent is absent, the ligand is in the anionic form (Figure 1B). With one exception, the reported solid-state complexes involving the neutral ligand and divalent transition metals are monomeric.[12−16] The exception is the dimeric complex $Ni_2(4\text{-aminobpt})_2(HOH)_2Cl_2$.[17]

Anionic forms of the ligand, on the other hand, are normally seen to bridge two metal atoms. When the pyridyl nitrogen atoms face in the same direction as the N1 and N2 positions (Figure 1B) and the four nitrogen atoms serve as bidentate ligands to two different metal atoms, metal−metal distances of about 4 Å are seen.[18] Bis[μ-3,5-bis(pyridin-2-yl)-1,2,4-triazolato-N',N^1,N^2,N'']bis[aqua(trifluoromethanesulfonato-*O*)copper(II)] displays this mode of bonding with axial ligation to a trifluoromethanesulfonato oxygen atom and the oxygen atom of a water molecule. Copper(II) atoms, separated by 4.085(1) Å, display antiferromagnetic interaction with singlet−triplet splitting of 204−236 cm^{-1}. Electron paramagnetic resonance (EPR) measurements demonstrated the existence of an excited triplet state with Cu−Cu hyperfine interactions at 77 K.[18] However, one pyridine ring may rotate 180° to bond to a metal atom along with the nitrogen atom in the 4 position. A second metal is found on the opposite side of the ligand bound to the nitrogen atom of the remaining pyridine ring and to the near nitrogen of the triazole ring.[19] In this case, metal atoms are widely separated.

We report here the single-crystal structure and EPR, thermogravimetric analysis (TGA), and magnetic characterization of the dimeric complex $Cu_2(bptd)Cl_4(HOH)$ over a range of temperatures.

Experimental Section

Synthesis. bptd was synthesized as described previously.[20] Copper(II) chloride dihydrate (1.5 mmol, 0.26 g) dissolved in 8 mL of hot water was added to 0.42 mmol (0.1 g) of the bptd ligand dissolved in 8 mL of hot ethanol. The solution was filtered and allowed to stand at ambient temperature. After 24 h, a green compound crystallized. Crystals were washed with water and dried under vacuum. These crystals were used as isolated for single-crystal X-ray analysis. The crystals isolated were ground to a fine powder, which was used for all of the other measurements.

Thermal Analysis. Coupled TGA and differential thermal analysis measurements were carried out with a Setaram 92-1600 apparatus using a 1 °C min^{-1} heating rate in an atmosphere of air. High-temperature powder X-ray diffraction (XRD) data were obtained using either a moving-film Guinier Lenne camera or a D5000 Siemens diffractometer equipped with a high-temperature stage.

Continuous Wave (CW) and Pulsed Electron Spin Resonance (ESR) Spectra. X-band ESR spectra were recorded with a Brüker ELEXYS 580 spectrometer operating at a 100 kHz modulation frequency and equipped with a nitrogen gas flow for temperature regulation. Spectra were recorded in the temperature range between 113 and 453 K. The pulsed ESR study was achieved using a 2D four-pulse HYSCORE (hyperfine sublevel correlation spectroscopy) sequence. HYSCORE measurements were carried out with the sequence $\pi/2-\tau-\pi/2-t_1-\pi-t_2-\pi/2-\tau$ echo and a four-step phase cycle. The pulse lengths of the $\pi/2$ and π pulses in these experiments were 12 and 24 ns, respectively. The τ value was 120 ns. Prior to the Fourier transformation of the HYSCORE data, background decay was removed by a polynomial fit.

(8) Lagrenée, M.; Sueur, S.; Wignacourt, J. P.; Mernari, B.; Boukhari, A. *J. Chim. Phys. Phys.-Chim. Biol.* **1991**, *88*, 2075−2082.
(9) Gueddi, A.; Mernari, B.; Giorgi, M.; Pierrot, M. *Acta Crystallogr.* **2000**, *56E*, E426−E428.
(10) Wignacourt, J. P.; Sueur, S.; Lagrenée, M. *Acta Crystallogr., Sect. C* **1990**, *46*, 394−396.
(11) Bentiss, F.; Lagrenée, M.; Wignacourt, J. P.; Holt, E. M. *Polyhedron* **2002**, *21*, 403−408.
(12) Van Koningsbruggen, P. J.; Goubitz, K.; Hassnoot, J. G.; Reedijk, J. *Inorg. Chim. Acta* **1998**, *268*, 37−42.
(13) Faulman, C.; Van Koningsbruggen, P. J.; de Graaf, R. A. G.; Hassnoot, J. G.; Reedijk, J. *Acta Crystallogr., Sect. C* **1990**, *46*, 2357−2360.
(14) Jircitano, A. J.; Sommerern, S. O.; Abboud, K. A. *Acta Crystallogr., Sect. C* **1997**, *53*, 434−436.
(15) Zhu, D.; Song, Y.; Liu, Y.; Xu, Y.; Zhang, Y.; You, X.; Raj, S. S.; Fun, H. K. *Transition Met. Chem.* **2000**, *25*, 589−593.
(16) Kunkeler, P. J.; Van Koningsbruggen, P. J.; Cornelissen, J. P.; Van der Horst, A. N.; Van der Kraan, A. M.; Spek, A. L.; Haasnoot, J. G.; Reedijk, J. *J. Am. Chem. Soc.* **1996**, *118*, 2190−2197.
(17) Keijj, F. S.; de Graaff, R. A. G.; Haasnoot, J. G.; Reedijk, J. *J. Chem. Soc., Dalton Trans.* **1984**, 2093−2097.
(18) Prins, R.; Birker, P. J. M. W. L.; Haasnoot, J. G.; Verschoor, G. C.; Reedijk, J. *Inorg. Chem.* **1985**, *24*, 4128−4133.
(19) Hage, R.; Haasnoot, J. G.; Nieuwenhuis, H. A.; Reedijk, J.; DeRidder, D. J.; Vos, A. J. G. *J. Am. Chem. Soc.* **1990**, *112*, 9245−9251.
(20) Mazzone, G.; Puglisi, G.; Bonina, F.; Corsaro, A. *J. Heterocycl. Chem.* **1983**, *20*, 1399−1401.

Table 1. Crystallographic Data and Details of the Data Collection for $Cu_2(bptd)Cl_4(HOH)$ at Room Temperature and at 100 K

	293 K	100 K
chemical formula	$C_{12}H_{10}Cl_4Cu_2N_4OS$	
formula weight (g/mol)	527.18	
a (Å)	9.296(3)	9.244(2)
b (Å)	9.933(3)	9.891(2)
c (Å)	10.412(3)	10.311(2)
α (deg)	79.054(5)	78.976(3)
β (deg)	82.478(6)	81.981(3)
γ (deg)	67.099(5)	67.233(3)
V (Å^3)	867.8(5)	851.0(3)
Z	2	
cell class	triclinic	
space group	$P\bar{1}$	
crystal color	green	
density calculated (g/cm^3)	2.017	2.057
F(000)	520	
abs coeff (mm^{-1})	3.194	3.257
radiation type (wavelength)	Mo Kα (0.710 73 Å)	
monochromator	graphite	
diffractometer	Brucker SMART	
reflns meas/independent/ obs param	3984/2473/2203;221	6174/3313/3193
average R equivalents	0.0278	0.226
index limits	$-10 < h < +7$	$-11 < h < +12$
	$-11 < k < +8$	$-12 < k < +13$
	$-11 < l < +11$	$-13 < l < +13$
$\theta_{min}/\theta_{max}$	2.60/23.29	2.26/28.23
reflns threshold expression	$I > 2\sigma(I)$	
refinement	F^2, full matrix	
weighting scheme	$A = 0.0968$	$A = 0.0370$
$w = 1/[(\sigma^2F_o^2) + (AP)^2 + BP]$ where $P = (F_o^2 + 2F_c^2)/3$	$B = 0.00$	$B = 2.7139$
R factor (all/gt)	0.0460/0.0428	0.0299/0.0289
wR factor (all/gt)	0.1203/0.1170	0.0690/0.0683
GOF	1.013	0.832
shift/error (max/mean)	0.008/0.000	4.624/0.021

Magnetic Susceptibility. Magnetic susceptibility was measured with a Quantum Design DC SQUID magnetometer over the range of 5−300 K. Zero-field-cooling (ZFC) and field-cooling (FC) data were measured with a 2500 Oe applied field on a 8.1×10^{-5} mole sample of the title compound. The data were corrected for molecular diamagnetism using the tabulated data of ref 21.

Crystallographic Data. A single crystal of $Cu_2(bptd)Cl_4(HOH)$ was mounted on a Brucker Smart three-circle diffractometer equipped with a CCD bidimensional detector set at 5 mm from the crystal. One hemisphere of data was collected with a 40 s acquisition time at room temperature (301 K). The crystal data are presented in Table 1. Data were corrected for background, Lorentz, and polarization effects[22] and for absorption.[23] The non-hydrogen positions were determined using SHELXL-97[24] and refined using full-matrix least-squares refinement[25] against F^2 values. Hydrogen atoms were positioned in idealized positions and included in the final cycles of refinement with fixed isotropic thermal parameters, yielding the final R1 = 4.6% and wR2 = 12.03% for all of the 2473 unique reflections. The final atomic positional parameters given in Table 2 are the basis for the bond distances and angles of Table 3. Anisotropic thermal parameters and hydrogen positional information are available as the Supporting Information. Low-temperature (T = 100 K) XRD data have been collected on the same system using an OXFORD CRYOSTREAM cooling device.

Table 2. Positional Parameters for $Cu_2(bptd)Cl_4(HOH)$ at Room Temperature

atom	$x[\sigma(x)]$	$y[\sigma(y)]$	$z[\sigma(z)]$	U_{equiv}
Cu1	0.637 28(6)	0.908 08(5)	0.351 45(5)	0.0306(2)
Cu2	0.284 19(6)	1.242 71(5)	0.236 29(5)	0.0297(2)
Cl1	0.203 10(13)	1.477 14(12)	0.261 90(11)	0.0395(3)
Cl2	0.425 61(13)	1.240 07(12)	0.010 78(10)	0.0384(3)
Cl3	0.510 53(12)	1.161 95(12)	0.355 89(10)	0.0350(3)
Cl4	0.852 21(13)	0.890 20(13)	0.434 18(12)	0.0429(3)
O1	0.7044(4)	0.9431(4)	0.1229(3)	0.0430(8)
S1	0.241 55(12)	0.810 43(12)	0.253 53(11)	0.0335(3)
C2	0.4211(5)	0.7879(5)	0.3000(4)	0.0259(9)
N3	0.4374(4)	0.9118(4)	0.2998(3)	0.0268(8)
N4	0.3120(4)	1.0313(4)	0.2588(3)	0.0285(8)
C5	0.1989(5)	0.9977(4)	0.2300(4)	0.0265(9)
C6	0.5582(5)	0.6530(5)	0.3389(4)	0.0269(9)
N7	0.6777(4)	0.6854(4)	0.3665(3)	0.0298(8)
C8	0.8081(5)	0.5747(5)	0.4048(4)	0.0353(10)
C9	0.8229(5)	0.4285(5)	0.4180(4)	0.0354(10)
C10	0.7024(5)	0.3964(5)	0.3870(4)	0.0344(10)
C11	0.5660(5)	0.5112(5)	0.3469(4)	0.0326(10)
C12	0.0612(5)	1.1212(5)	0.1787(4)	0.0290(9)
N13	0.0758(4)	1.2528(4)	0.1735(3)	0.0282(8)
C14	−0.0393(5)	1.3744(5)	0.1235(4)	0.0342(10)
C15	−0.1708(5)	1.3712(5)	0.0776(4)	0.0393(11)
C16	−0.1858(5)	1.2381(5)	0.0860(4)	0.0399(11)
C17	−0.0683(5)	1.1092(5)	0.1383(4)	0.0332(10)

Structure refinement was carried out in the same way, leading to R1 = 2.99% and wR2 = 6.90% for all of the 3313 unique reflections. No significant atomic shift was observed from the room-temperature crystal structure. Crystal data and pertinent bond distances and angles from the low-temperature refinement are presented in Tables 1 and 3.

Computational Chemistry. Computations were performed with Gaussian98 software using the density functional theory and DFT B3LYP/6-31+G(2d,2p) formalism.[26] A single-point energy calculation was done on the basis of crystallographic data for the singlet and triplet states using a high self-consistent-field calculation.

Results

Crystal Structure at Room Temperature. At room temperature, $Cu_2(bptd)Cl_4(HOH)$ exists as a dimer of copper atoms separated by a distance of 3.7800(8) Å (Figure 2). The copper atoms are bridged by a Cl [average Cu−Cl = 2.3539(13) Å; Cu1−Cl3−Cu2 = 106.81(4)°] and the tetradentate 2,5-bis(2-pyridyl)-1,3,4-thiadiazole ligand. Each copper atom is bound to one nitrogen atom of the thiadiazole ring [average Cu−N = 1.985(3) Å] and the adjacent pyridyl nitrogen atom [average Cu−N = 2.079(4) Å].

The atoms of the bptd ligand are coplanar (standard deviation = 0.07), and the copper atoms lie on that plane within the experimental error. The bridging chloride atom Cl3 is displaced 0.546 Å above the equatorial plane as are

(21) Kahn, O. *Molecular Magnetism*; Wiley-VCH: New York, 1993.
(22) *SAINT: Area Detector Integration Software*; Siemens Industrial Automation, Inc.: Madison, WI, 1995.
(23) *SADABS: Area Detector Absorption Correction*; Siemens Industrial Automation, Inc.: Madison, WI, 1996.
(24) Sheldrick, G. M. *Acta Crystallogr., Sect.* A **1990**, *46*, 467−472.
(25) Sheldrick, G. M. *SHELXL-97: Program for the Refinement of Crystal Structures*; University of Gottingen: Gottingen, Germany, 1997.
(26) Frisch, M. J.; Trucks, G. W.; Schlegel, H. B.; Scuseria, G. E.; Robb, M. A.; Cheeseman, J. R.; Zakrzewski, V. G.; Montgomery, J. A.; Stratmann, R. E., Jr.; Burant, J. C.; Dapprich, S.; Millam, J. M.; Daniels, A. D.; Kudin, K. N.; Strain, M. C.; Farkas, O.; Tomasi, J.; Barone, V.; Cossi, M.; Cammi, R.; Mennucci, B.; Pomelli, C.; Adamo, C.; Clifford, S.; Ochterski, J.; Petersson, G. A.; Ayala, P. Y.; Cui, Q.; Morokuma, K.; Malick, D. K.; Rabuck, A. D.; Raghavachari, K.; Foresman, J. B.; Cioslowski, J.; Ortiz, J. V.; Baboul, A. G.; Stefanov, B. B.; Liu, G.; Liashenko, A.; Piskorz, P.; Komaromi, I.; Gomperts, R.; Martin, R. L.; Fox, D. J.; Keith, T.; Al-Laham, M. A.; Peng, C. Y.; Nanayakkara, A.; Challacombe, M.; Gill, P. M. W.; Johnson, B.; Chen, W.; Wong, M. W.; Andres, J. L.; Gonzalez, C.; Head-Gordon, M.; Replogle, E. S.; Pople, J. A. *GAUSSIAN98*, revision A.9; Gaussian, Inc.: Pittsburgh, PA, 1998.

Table 3. Selected Distances (Å) and Bond Angles (deg) for $Cu_2(bptd)Cl_4(HOH)$

organic distances (room temperature)		organic angles (room temperature)	
S1−C2	1.718(4)	C2−S1−C5	87.1(2)
S1−C5	1.719(4)	N3−C2−C6	115.4(4)
C2−N3	1.297(5)	N3−C2−S1	113.4(3)
C2−C6	1.478(6)	C6−C2−S1	131.1(3)
N3−N4	1.346(5)	C2−N3−N4	113.2(3)
N4−C5	1.304(5)	C5−N4−N3	113.1(3)
C5−C12	1.462(6)	N4−C5−C12	116.4(4)
C6−N7	1.348(5)	N4−C5−S1	113.1(3)
C6−C11	1.368(6)	C12−C5−S1	130.4(3)
N7−C8	1.326(5)	N7−C6−C11	123.0(4)
C8−C9	1.386(6)	N13−C12−C5	111.5(3)
C9−C10	1.369(6)	C17−C12−C5	125.6(4)
C10−C11	1.384(6)	C14−N13−C12	117.6(4)
C12−N13	1.356(5)	N13−C14−C15	122.9(4)
C12−C17	1.380(6)	C16−C15−C14	118.9(4)
N13−C14	1.332(5)	C15−C16−C17	119.7(4)
C14−C15	1.383(6)	C12−C17−C16	117.9(4)
C15−C16	1.367(7)	Cu1−Cl3−Cu2	106.81(4)
C16−C17	1.390(6)	Cu1−N3−N4	127.6(3)
		Cu2− N4−N3	128.6(4)

		angles (room temperature)			
	Cu1 distance	N3	N7	Cl4	Cl3
N3	1.983(3)				
N7	2.072(4)	77.36(13)			
Cl4	2.209(1)	172.59(10)	99.44(9)		
Cl3	2.338(1)	87.09(10)	161.57(10)	94.78(4)	
O1	2.371(3)	85.76(12)	95.71(12)	101.29(8)	92.92(9)

		angles (100 K)			
	Cu1 distance	N3	N7	Cl4	Cl3
N3	1.979(2)				
N7	2.065(2)	77.81(9)			
Cl4	2.2085(8)	172.53(7)	99.30(7)		
Cl3	2.3336(8)	86.78(7)	161.80(7)	94.78(3)	
O1	2.339 (2)	85.44(8)	95.93(8)	101.78(5)	92.40(5)

		angles (room temperature)			
	Cu2 distance	N4	N13	Cl1	Cl3
N4	1.9842(34)				
N13	2.084 (3)	77.33(13)			
Cl1	2.208(1)	162.91(10)	96.86(10)		
Cl3	2.369(1)	86.38(10)	160.53(10)	95.69(4)	
Cl2	2.536(1)	93.80(10)	95.44(9)	102.81(4)	96.23(5)

		angles (100 K)			
	Cu2 distance	N4	N13	Cl1	Cl3
N4	1.9800(24)				
N13	2.075 (2)	77.69(9)			
Cl1	2.2093(8)	163.41(7)	96.67(7)		
Cl3	2.3535(8)	86.39(7)	161.36(7)	95.94(3)	
Cl2	2.5342(9)	93.59(7)	95.06(6)	102.50(3)	95.56(3)

the terminal chloride atoms Cl4 and Cl1 (displacements = 0.231 and 0.640 Å, respectively).

The two copper atoms are not equivalent because Cu2 is axially bonded to Cl2 [Cu2−Cl2 = 2.5358(13) Å], whereas Cu1 is bonded axially to the oxygen of a water molecule [Cu1−O1 = 2.375(3) Å]. Considering only these interactions, one would identify the geometry at each copper(II) atom to be approximately square pyramidal. However, examination of the packing shows the dimeric complex to have distant Cu−Cl interactions, with a second complex related by a center of symmetry [Cu1···Cl3 ($1 - x$, $2 - y$, $1 - z$) = 3.240(1) Å and Cu2···Cl4 ($1 - x$, $2 - y$, $1 - z$) = 3.680(1) Å, thus completing the distorted octahedral around both Cu1 and Cu2].

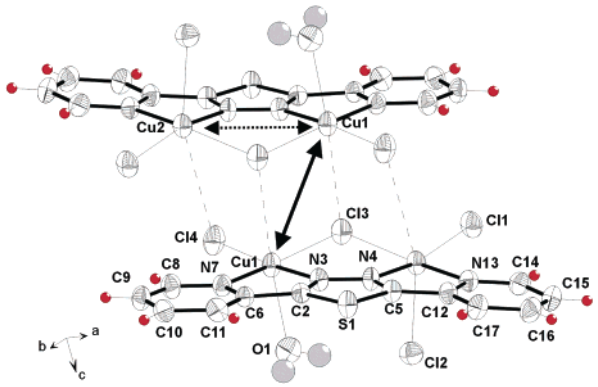

Figure 2. View of the dimeric complex μ-chloro-μ-[2,5-bis(2-pyridyl)-1,3,4-thiadiazole] aqua chlorocopper(II) dichlorocopper(II).

An attempt at validation of these distant interactions using a bond valence approach reveals that the contributions of the distant chloride ions to the valence total are minimal (0.035 and 0.011 for Cl3···Cu1 and Cl4···Cu2, respectively). The strongest argument for the validity of these distant interactions is seen in the geometry at copper. The copper atom is coplanar with its equatorial plane of N3−N7−Cl3−Cl4 and N4−N1−Cl1−Cl3 for Cu1 and Cu2, respectively. It is not displaced from that plane toward the axial ligand as is typical for square-pyramidal geometry. Furthermore, the angles at copper between the axial ligand and the distant chloride neighbor [167.5(4) and 160.4(4)° for Cu1 and Cu2, respectively] are appropriate for the distorted-octahedral geometry.

The dimeric complexes of $Cu_2(bptd)Cl_4(HOH)$ are packed in the unit cell, with copper and bptd ligand lying on the (103) planes. Interaction between the dimeric moieties occurs between these layers. Water molecules and Cl2 atoms are found on intervening (103) planes. Inter- and intracomplex hydrogen bondings occur between the protons of the water molecule and Cl2 [H1A−Cl2 ($1 - x$, $2 - y$, $-z$) = 2.712 Å; H1B−Cl2 = 2.337 Å]. It is noteworthy that interlayer interactions involve two dimeric clusters related by a center of symmetry and with Cl4 and Cl3 forming links between them. The Cl2 and OH_2 apical ligands of each cluster point away from the neighboring clusters. The interaction between pairs of neighboring clusters is responsible for the particular magnetic properties described below. Figure 2 shows the numbering scheme and displays the particular interactions that exist within pairs of $Cu_2(bptd)Cl_4(HOH)$ molecules. The arrows point out the competing intra- and intermolecular Cu−Cu interactions.

Comparison of the powder spectrum calculated on the basis of the single-crystal structure with the experimental pattern of the powder sample used for other measurements shows that the two spectra correspond and thus indicates the homogeneity of the powder and its structural identity with the single crystal.

The single-crystal examination at 100 K verified the identity of the low-temperature solid-state structure with that

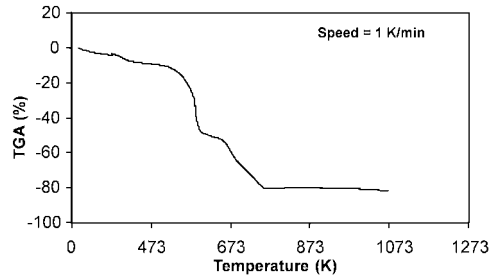

Figure 3. Thermal evolution of $Cu_2(bptd)Cl_4(HOH)$.

seen at room temperature in an identical space group and in agreement of the atomic positional parameters. The low-temperature unit-cell dimensions [$a = 9.244(2)$ Å, $b = 9.891(2)$ Å, $c = 10.311(2)$ Å, $\alpha = 78.976(3)°$, $\beta = 81.981(3)°$, $\gamma = 67.233(3)°$] compared to the room-temperature cell dimensions show a maximum contraction of the *c* axis (0.97%) compared to the room-temperature cell dimensions (versus 0.56 and 0.43% for *a* and *b*, respectively). Shrinkage of the *c* axis, which is almost parallel to the intermolecular stacking axis, leads to a slight shortening of coupled intercluster distances, while intramolecular covalent bonds remain nearly unchanged.

Thermal Analysis at Temperatures above the Ambient. The thermal evolution of $Cu_2(bptd)Cl_4(HOH)$ has been studied both by TGA and high-temperature XRD, using a Guinier Lenne camera. TGA shows a loss of mass between room temperature and 348 K (Figure 3); the weight loss of 3.3% accounts for 1 mol of OH_2/mol of complex (H_2O theoretical = 3.41%). High-temperature XRD shows a change in pattern in the same temperature range. TGA shows a second loss of about 7% of the weight of the remaining mass between 348 and 423 K. In this temperature range, the diffraction pattern is observed to be a superposition of the pattern of the dehydrated species seen at 348 K (vanishing) and a new one (forming progressively). This can be interpreted as the loss of 1 mol of Cl/mol of complex (theoretical = 6.97%). The diffraction pattern of that "new" phase is then observed unchanged of up to 523 K, and this is verified by a corresponding weight stabilization in the TGA spectrum. Above 533 K, the diffraction pattern is that of an amorphous material. The TGA plot above 533 K shows a significant weight loss corresponding to the ligand decomposition, which is accompanied by a strong exothermal effect. Exothermal activity is completed around 773 K, yielding a residue (about 18% of the initial weight) identified as CuO upon cooling to room temperature. A microprobe quantitative analysis of an independent sample heated to 433 K for 12 h corroborates the loss of 1 mol of H_2O and 1 mol of Cl/mol of complex, leaving the residual $Cu_2(bptd)Cl_3$ at that temperature.

ESR (50−350 K). Figure 4 displays the ESR spectra of $Cu_2(bptd)Cl_4(HOH)$, measured on crushed crystals at 77 K. It shows a broad axial symmetrical signal with $g_{\parallel} = 2.27$ and $g_{\perp} = 2.07$, consistent with a $d_{x^2-y^2}$ orbital ground state. However, no transition resulting from the magnetic interaction between the two copper ions was observed even though crystallographic data agree on a Cu−Cu separation of 3.78 Å. The response of the ESR signal change in temperature has been studied. The plot of the double integral of the ESR signal versus *T* displays the profile of a paramagnetic compound according to the Curie−Weiss law (Figure 5). This profile appears to show a change in slope close to 140 K. In as much as the low-temperature single-crystal structure appears unchanged, this evolution must represent an electronic rearrangement and not a structural one.

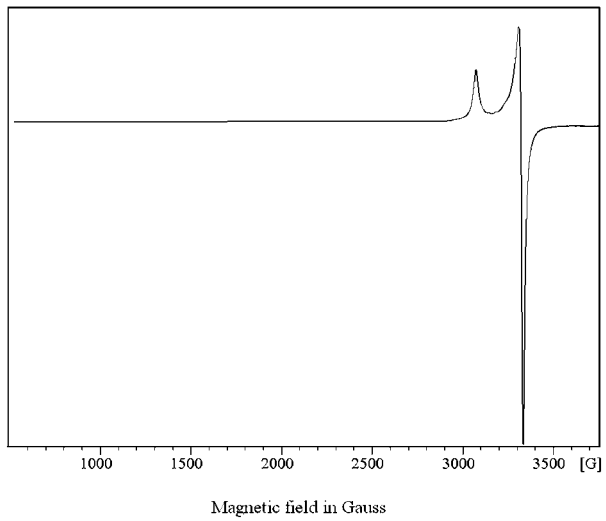

Figure 4. X-band powder ESR spectrum of $Cu_2(bptd)Cl_4(HOH)$ at 77 K. Experimental settings were amplitude modulation = 5 G and microwave power = 5 mW.

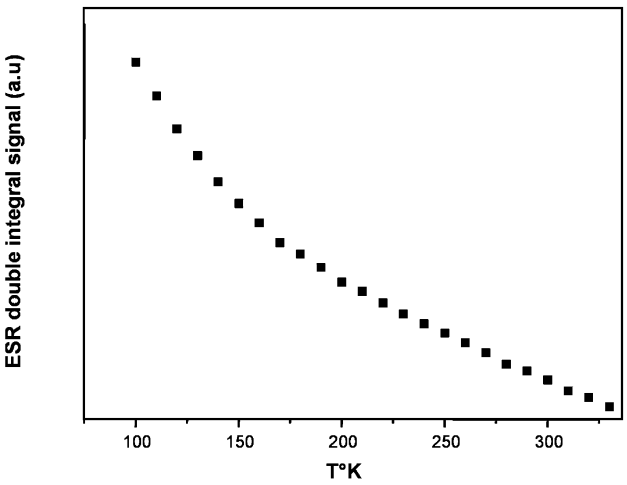

Figure 5. Double integral of the ESR signal versus *T*.

Magnetism (3−300 K). Parts a and b of Figure 6 show respectively the molar χT product and the χ^{-1} versus temperature plots for $Cu_2(bptd)Cl_4(OH_2)$. ZFC and FC data show a good reversibility. Two linear components separated by a change in slope at $T_t = 125$ K are observed on the χ^{-1} plot. Despite the temperature difference, this phenomenon is likely related to the above-mentioned phenomenon observed from the ESR data. From room temperature to T_t, χ_m^{-1} versus *T* can be fitted by a Curie−Weiss law: $\chi_m^{-1} = (T - \theta_{CW})/C_m$, with $C_m = 0.707$ K/emu and $\theta_{CW} = -166.4$ K. It leads to $\mu_{eff} = 2.37$ μ_B/fu matching well with the theoretical 2.44 value in a spin-only approximation. In fact, one should consider in this thermal range the progressive

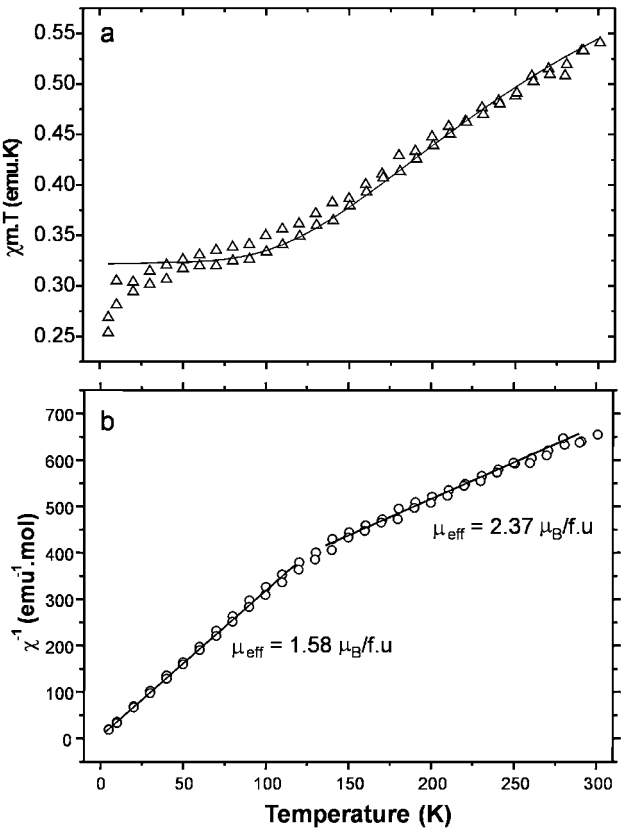

Figure 6. (a) χT and (b) χ^{-1} versus temperature for $Cu_2(bptd)Cl_4(HOH)$. The solid line in part a corresponds to the calculated values from data of the Bleaney−Bowers fit.

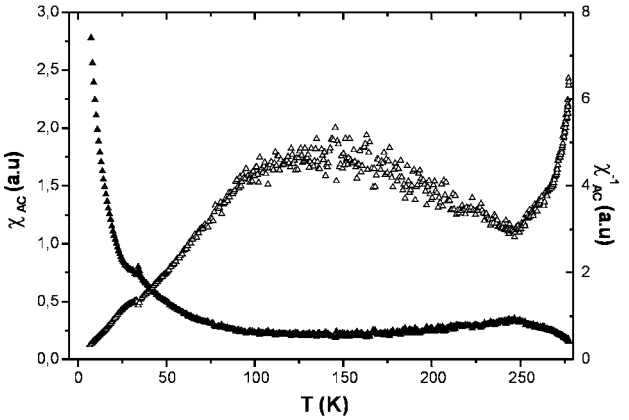

Figure 7. χ_{ac} and χ_{ac}^{-1} versus T, with a null dc offset field (H_{ac} = 40 Oe). χ_{ac} obeys a Curie−Weiss law below 110 K. The χ_{ac}^{-1} plateau at higher temperatures shows the Cu1−Cu1 antiferromagnetic exchange setting.

settings of dinuclear interactions, which concern only a part of the copper cations, with the other part remaining paramagnetic in the complete temperature range. The negative sign of θ_{CW} indicates antiferromagnetic correlations between Cu^{2+} ions, but questions remain about the low-temperature domain. Effectively, below T_t, χ_m^{-1} obeys a Curie−Weiss law with $\chi_m^{-1} = T/C_m$, yielding C_m = 0.315 K/emu (μ_{eff} = 1.58 μ_B/fu), which is slightly smaller than a single Cu^{2+} contribution (μ_{eff} theoretical = 1.73 μ_B/fu) in a spin-only approximation. This phenomenon is also observed in Figure 7, which shows χ_{ac} and χ_{ac}^{-1} versus T with a null dc offset field (H_{ac} = 40 Oe, f = 1013 Hz). Below 110 K, χ_{ac}^{-1} obeys

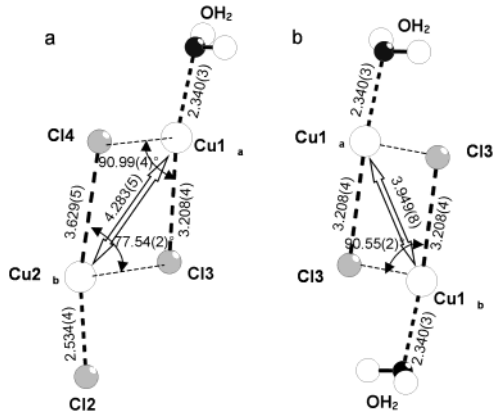

Figure 8. View of possible interactions between the dimeric units completing the octahedral geometry of the copper atoms. Only the Cu1−Cl3−Cu1 superexchanges would remain Cu2 paramagnetic at low temperatures.

a Curie−Weiss law, while a broad plateau is observed above, which could correspond to dimeric interactions as detailed below. It is noteworthy that an additional weak phenomenon appears around 35 K, which is currently under investigation.

First of all, considering the nearly unchanged crystal structure at 100 K, the observed magnetic behavior is intrinsic to the refined model. Thus, intradimer Cu1−Cu2 couplings are not observed, i.e., because one of the copper(II) atoms of the dimer retains a paramagnetic character at low temperatures. It is then necessary to involve intermolecular magnetic exchange in good agreement with the particular packing involving pairs of dinuclear complexes related by the center of symmetry. Considering the Cu−Cu distances and angles possibly intervening in the magnetic pathway for intermolecular exchanges, it appears that two different couplings compete as shown in Figure 8a,b.

i. $Cu1_a$−$Cu2_b$ (where the a and b indices stand for two distinct molecules) involves a Cu−Cu distance of 4.283(5) Å, which is too long for direct interaction. At least, the possibility of antiferromagnetic Cu1−Cl4−Cu2 and Cu1−Cl3−Cu2 exchanges exists considering the engaged angles (Figure 8a). For symmetrical reasons, two $Cu1_a$−$Cu2_b$ and $Cu1_b$−$Cu2_a$ couplings would occur within pairs of molecules, contradicting the paramagnetic behavior at low temperatures.

ii. $Cu1_a$−Cl3−$Cu1_b$ superexchanges are more likely to occur considering the relatively short distance [d = 3.949(8) Å] and the two Cu1−Cl3−Cu1 angles of 90° involved (Figure 8b). It is noteworthy that the maximal lattice parameter contraction on cooling involves the c axis, which corresponds to the intermolecular packing axis. So, the T_t is assigned to the intermolecular Cu1−Cu1 antiferromagnetic setting, while the remaining P_{eff} of 1.58 μ_B/fu is assigned to the Cu2 paramagnetic contribution. This coupling involves the Cu1 magnetic electron existing in the d_{z^2} orbital, while the 77 K ESR spectrum indicates that the paramagnetic Cu2 electron has $d_{x^2-y^2}$ characteristics. The square Cu1−Cl3−Cu1−Cl3 path involving only 90° angles should imply double-correlation superexchanges: e_g−p_σ−p_σ'−e_g, where p_σ and p_σ' are two perpendicular orbitals of the chloride anion.

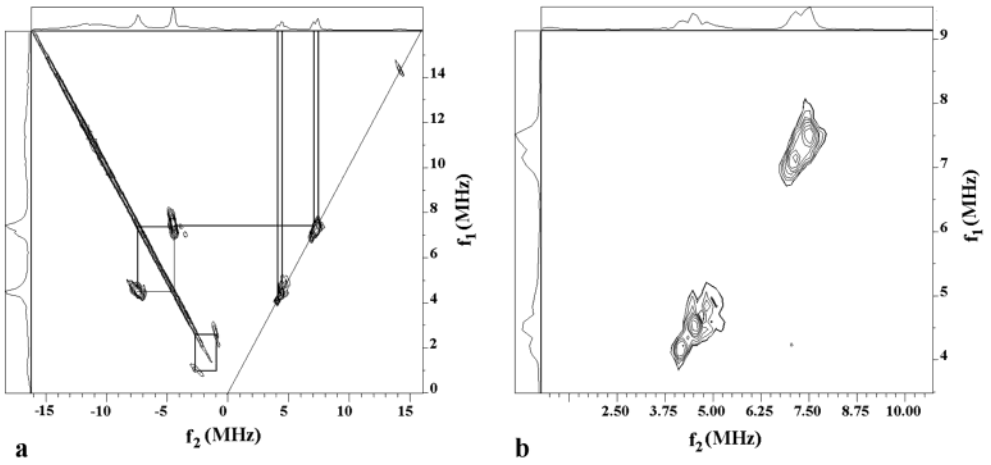

Figure 9. 2D HYSCORE spectrum of the powder solid state of $Cu_2(bptd)Cl_4(HOH)$ recorded at $B_0 = 332$ mT ($g_\perp$ region), $\tau = 156$ ns, and $T = 4.2$ K: (a) full spectrum; (b) onset zoom of the (+, +) quadrant.

The χT data have been fitted according to the Bleaney−Bowers equation that describes dinuclear interactions derived from the $H = -2JS_1S_2$ Hamiltonian. This equation was modified considering f % of coupled Cu^{2+} (namely, Cu1) assigned to g_1 and the $(1 - f)$ % ratio of paramagnetic Cu^{2+} cations (namely, Cu2) assigned to g_2

$$\chi_m = \frac{N\beta^2 g_1^{\,2}}{3kT}\left[1 + \frac{1}{3}\exp(-2J/kT)\right]^{-1}(f) + \frac{(N\beta^2 g_2^{\,2})(1-f)}{4kT} + N_\alpha$$

$2J$ is the singlet−triplet splitting and N_α is the temperature-independent paramagnetism. A nonlinear regression analysis on χT with g_1, g_2, J, and N_α as the variables roughly converged. g_1 and g_2 have been fixed to 2.05, yielding $f =$ 40.3(2)%, $-J = 180(2)$ cm^{-1}, $N_\alpha = -0.000\,04(1)$ emu, and $\chi^2 = 2.3 \times 10^{-4}$. The f deviation from its expected 50% value may be due to the slight divergence between the ZFC and FC data. The J value comforts the strong antiferromagnetic coupling between the intermolecular Cu1 copper centers. The calculated data are represented by the solid line of Figure 6a.

Pulsed ESR. To confirm the suggested model, the title compound was also investigated by pulsed ESR spectroscopy using a 2D four-pulse HYSCORE sequence at 4.2 K. A four-pulse HYSCORE experiment[27,28] measures the energy splittings of nuclei whose spins interact with the spin of unpaired electrons. The 2D contour plot HYSCORE spectrum displayed in Figure 9a shows a weak proton coupling centered at the ^{1}H Larmor frequency of 14.5 MHz on the (+, +) quadrant. This ^{1}H frequency can be easily assigned to the protons of the H_2O group bonded to Cu1. The weakness of this coupling is in good agreement with the Cu2-only paramagnetism response at this temperature involving Cu2−N−N−Cu1−OH_2 bridges. The strong anisotropic feature observed in the negative f_2 quadrant is due to the second copper nucleus, namely, Cu1. The strong correlation pattern observed at approximately (+4.3, −7.2) and (+7.2, −4.3) MHz in the negative quadrant can be assigned to the $\nu_{dq\pm}$ of the ^{14}N nuclei coupled to Cu2. These frequencies of 4.3 and 7.2 MHz, respectively, were also observed in the diagonal of the positive (+, +) quadrant with a cross-peak correlation pattern. It can be observed in the onset expansion (Figure 9b) that these peaks are both formed by a doublet of two separate frequencies with a difference of 0.4 MHz. These results indicate that the four ^{14}N nuclei surrounding the two copper atoms are nonequivalent in pairs of two, agreeing with the structural data [N13−N4 (Cu2) and N3−N7 (Cu1)]. Moreover, an additional correlation pattern is observed at approximately (+0.90, −2.2) and (+2.2, −0.9) MHz in the negative quadrant that can be attributed to the single quantum $\nu_{sq\pm}$ of coupled ^{14}N.

Computational Chemistry. To verify the lack of intramolecular coupling between the two copper ions, theoretical calculations using density functional theory have been performed. Calculations of the single-point energy of both singlet and triplet states show a very small singlet−triplet gap energy of 0.5 cm^{-1}, in good agreement with our model. Moreover, the spin-density analysis confirms two different situations as follows: for Cu1, a localization is seen on the d_{z^2} orbital, whereas the Cu2 spin density remains preferentially on the $d_{x^2-y^2}$ orbital. It also shows that the two nitrogen atoms bonding Cu1 (N3 and N7) have a small positive spin-density value, whereas those on Cu2 (N13 and N4) have a strong negative value. These results can be related to the observed HYSCORE correlation pattern.

Discussion and Conclusions

The magnetic properties of the title compound contradict the behavior observed for a number of related complexes with M−N−N−M diazole (or related) bridges in planar dinuclear molecules, yielding more or less strong antiferromagnetic couplings.

A number of such compounds have been characterized with different ligands and metals. It has been observed that

(27) Höfer, P. *J. Magn. Reson., Ser. A* **1994**, *111*, 77−82.
(28) Höfer, P.; Grupp, A.; Nebenführ, H.; Mehring, M. *Chem. Phys. Lett.* **1986**, *132*, 279−284.

for diazine or double diazine ligands [3,5-bis(2-pyridyl)-1,2,4-triazole (bpt)/3,5-bis(2-pyridyl)-4-amino-1,2,4-triazole (abpt); 1,4-dicarboxylatopyridazine (dcpz); 1,4-dihydrazinophtalazine (dhph)] the superexchange values are all in the order $J_{Cu-Cu} \gg J_{Ni-Ni} \gg J_{Co-Co}$, thus reinforcing the particular interest in our copper compound.[29] Other examples are reported, such as $[Cu_2(pt)_2(SO_4)(H_2O)_3](H_2O)_3$, with $J = -49$ cm^{-1} [30] or a wide series of bis[μ-4-amino-3,5-bis(aminomethyl)-1,2,4-triazole-N',N^1,N^2, N''] (aamt) complexes that systematically show a $J \sim -100$ cm^{-1}, independent of the identity of the axially bonded molecules.[31] One cannot ignore the significant effect of the bridging chloride anions on the magnetic properties. Even if strong antiferromagnetic couplings are observed for a series of double-bridged copper pairs (both diazine and hydroxy bridges) with L = MIP, DPPN, PAP, apically bonded by Cl^- [e.g., $J = -400$ cm^{-1} for $Cu_2(MIP)(OH)Cl_3(H_2O)\cdot H_2O$,[32] weak J values characterize $Ni_2(abpt)_2Cl_2(H_2O)_2Cl_2\cdot 4H_2O$ with double diazine bridges and apical Cl^-, $J = -12.5$ cm^{-1},[33] and Cu_2(*trans*,*trans*-pmk)-Cl_4 with trans Cu−N−N−Cu bridges,[34] $J = -26$ cm^{-1}]. Furthermore, bridging chlorides such as Cl3 in the title compound play a key role. Recently, in monochloro-bridged complexes $[Cu_2(\mu\text{-}Cl)(L)_2](ClO_4)_3$, weak effects are observed [ferromagnetic for L_1 = 1,4-bis(pyridin-2-ylmethyl)-1,4-diazacycloheptane and antiferromagnetic for L_2 = 1,4-bis-(imidazol-4-ylmethyl)-1,4-diazacycloheptane].[35] For both compounds, it indicates that the magnetic electrons lie perpendicular to the organic plane as observed for Cu1 in the title compound. Doubly chloro-bridged copper dimers such as $Cu_2Cl_4(C_7H_7N_3)_4$ [36] and Cu_2(medpco-2H)Cl_2,[37] where medpco = *N*,*N*′-bis(2-*N*,*N*′-dimethylaminoethyl)pyridine-2,6-dicarboxamide, also show particular magnetic couplings, with a weak ferromagnetism for the former ($J = 3.5$ cm^{-1}) and no magnetic coupling for the latter despite short Cu−Cu separations. The Cl role may be seen as a distorting agent of the bridging geometry from planarity. For example, in polymeric Cu(bpo)Cl_2,[8] copper atoms are separated by 5.55 Å and bridged in series only by bpo ligands. Chloride atoms occupy axial positions in a terminal fashion. The oxadiazole ring is planar (standard deviation = 0.0018), but the two- and five-substituted 2-pyridyl rings each subtend an angle of 10.4° with the central ring. The magnetic behavior of this molecule indicates the absence of interaction between the Cu atoms, even if both the nonplanarity and the rather long Cu−Cu distance may play a role. In the tetrameric [Cu(μ-(3-(2-pyridyl)-5-(2-pyrazinyl)-1,2,4-triazole))$(HOH)]_4(NO_3)_4$-$(HOH)_{12}$ complex, the anionic triazole ring is coplanar with the substituted pyrazinyl and pyridyl rings, which comprise the bridging ligand.[18] Copper atoms are displaced 0.11 Å from the plane of the tetradentate ligand. Cu−Cu separations are on the order of 4.268−4.319 Å. Magnetic measurements show a weak antiferromagnetic interaction ($J = -0.5$ to -1.0 cm^{-1}).

Two other structures with bridging chloride atoms allow evaluation of the influence of a bridging chloride atom.

Polymeric Cu(1,3-bis[3-(5-amino-1,2,4-triazolyl)]triazene)-chloride crystallizes with a triazene linking two amino-substituted triazole units.[38] This planar molecule serves as a tridentate ligand to one copper(II) atom, and this along with bonding to the chloride atom [2.268(2) Å] establishes an equatorial plane. The copper is further bonded to the chloride atom of a neighboring copper atom {[Cu−Cl = 2.586(2) Å], [Cu−Cu = 3.5874(2) Å], [Cu−Cl−Cu = 95.06(7) Å]}. There is no ligand trans to the axial Cu−Cl bond. $J = -0.5$ to -1.0 cm^{-1}, indicating weak antiferromagnetic coupling between the copper atoms. These authors report that the largest J values are shown by complexes with large Cu−Cl−Cu angles and by compounds with large deviations from 180° of the angle X−Cu−L (L being the ligand trans to the bridging halide atom). The Cu−Cl−Cu angle of 95.06° observed was thought to lead to a poor effective overlap of the $d_{x^2-y^2}$ magnetic orbitals of the adjacent units.

Prins et al. have studied three trimeric complexes $[Cu_3(attn)_2(H_2O)_2Cl_2]Cl_4(H_2O)_4$, $[Cu_3(attn)_2(ZnCl_4)_2Cl_2](H_2O)_4$, and $[Cu_3(attn)_2(H_2O)_2Br_2]Br_4(H_2O)_4$ [attn = 1,9-bis(3-amino-4*H*-triazol-5-yl)-3,7-diathianone], with successive pairs of copper atoms bridged by two triazole units and a chloride atom.[39] Cu−Cu = 3.5426(1)−3.620(3) Å, Cu−Cl−Cu = 80.6(1)−84.013(9) Å, and Cl−Cu−trans ligand = 164.5(1)−167.07(3) Å. The equatorial plane comprised two sulfur and two nitrogen atoms of the ligand and contains the copper atoms (sum of the angles at copper = 359.84−360.2°). In these complexes, in which the conditions of coplanarity of equatorial ligands and a Cu−Cl−Cu angle of less than 90° establish an effective exchange pathway, strong intramolecular antiferromagnetic interaction is seen ($J = -70.9$ to -75.1 cm^{-1}).

In the title structure, the Cu−Cl−Cu angle is large [106.81(4)°]; the angles at copper between the bridging ligand and the trans neighbor are significantly reduced from 180° [Cl3−Cu1−N7 = 161.55(10)° and Cl3−Cu2−N13 = 160.51(10)°], but the bridging chloride atom is part of the equatorial plane. The irregularity of the geometry at copper is evident from the displacement of the bridging chloride atom by 0.546 Å from the plane of the copper atoms and the organic ligand. This irregularity may be reflected by the

(29) Escuer, A.; Vicente, R.; Mernari, B.; El Gueddi, A.; Pierrot, M. *Inorg. Chem.* **1997**, *36*, 2511−2516.
(30) Slangen, P. M.; Van Koningsbruggen, P. J.; Goubitz, K.; Haasnoot, J. G.; Reedijk, J. *Inorg. Chem.* **1994**, *33*, 1121−1126
(31) Koomen-Van Oudenniel, W. M. E.; de Graff, R. A. G.; Haasnoot, J. G.; Prins, R.; Reedijk, J. *Inorg. Chem.* **1989**, *28*, 1128−1133.
(32) Thompson, L. K.; Hartstock, F. W.; Robichaud, P. *Can. J. Chem.* **1984**, *62*, 2755−2762.
(33) Keij, F. S.; de Graaff, R. A. G.; Haasnoot, J. G.; Reedijk, J. *J. Chem. Soc., Dalton Trans.* **1984**, 2093−2097.
(34) O'Connor, C. J.; Romananch, R. J.; Robertson, D. M.; Eduok, E. E.; Fronczek, F. R. *Inorg. Chem.* **1983**, *22*, 449−454.
(35) Du, M.; Guo, Y.; Bu, X.; Ribas, J.; Monfort, M. *New J. Chem.* **2002**, *26*, 939−945.
(36) Skorda, K.; Bakalbassis, E. G.; Mrozinski, J.; Perlepes, S. P.; Raptopouloo, C. P.; Terzis, A. *J. Chem. Soc., Dalton Trans.* **1995**, 2317−2319.
(37) Antolovich, M.; Phillips, D. J.; Rae, A. D. *Inorg. Chim. Acta* **1995**, *230*, 139−144.
(38) Hanot, V. P.; Robert, T. D.; Kolnaar, J. J. A.; Hasnoot, J. G.; Kooijman, H.; Spek, A. L. *Inorg. Chim. Acta* **1997**, *256*, 327−329.
(39) Prins, R.; Biagini-Cingi, M.; Drillon, M.; deGraff, R. A. G.; Haasnoot, J. G.; Manotti-Lanfredi, A. M.; Rabu, P.; Reedijk, J.; Ugozzoli, F. *Inorg. Chim. Acta* **1996**, *248*, 35−44.

lack of intramolecular interaction, while intermolecular couplings occur between the Cu1 cations of pairs of stacked molecules (from room temperature to 125 K, the compound is paramagnetic, and at lower temperatures, both susceptibility and EPR measurements show the antiferromagnetic coupling of half of the Cu^{2+} ions, while the others stay paramagnetic.

Supporting Information Available: Hydrogen positional and anisotropic thermal parameters for $Cu_2(bptd)Cl_4(HOH)$ and a CIF file of the crystal geometry with selected bond lengths and angles of μ-chloro-μ-[2,5-bis(2-pyridyl)-1,3,4-thiadiazole] aqua chlorocopper(II) dichlorocopper(II). Crystal structure determination has been sent to the Cambridge Crystallographic Data Center, 12 Union Road, Cambridge CB2 1EZ, U.K., as CCDC183341 and can be obtained by contacting the CCDC (quoting the article details and the corresponding SUP number). This material is available free of charge via the Internet at http://pubs.acs.org.

IC030128S